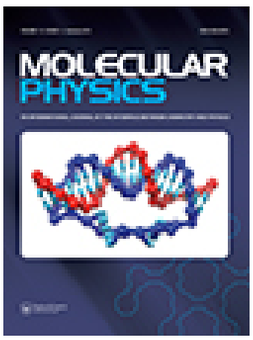

Taylor & Francis
Taylor & Francis Group

Molecular Physics

An International Journal at the Interface Between Chemistry and Physics

ISSN: 0026-8976 (Print) 1362-3028 (Online) Journal homepage: http://www.tandfonline.com/loi/tmph20

DNA nanotechnology: understanding and optimisation through simulation

Thomas E. Ouldridge

To cite this article: Thomas E. Ouldridge (2015) DNA nanotechnology: understanding and optimisation through simulation, Molecular Physics, 113:1, 1-15, DOI: 10.1080/00268976.2014.975293

To link to this article: http://dx.doi.org/10.1080/00268976.2014.975293

Published online: 24 Nov 2014.

Molecular Physics, 2015
Vol. 113, No. 1, 1–15, http://dx.doi.org/10.1080/00268976.2014.975293

Taylor & Francis
Taylor & Francis Group

NEW VIEW

DNA nanotechnology: understanding and optimisation through simulation

Thomas E. Ouldridge[a,b,*]

[a]*Rudolf Peierls Centre for Theoretical Physics, Physics Department, University of Oxford, Oxford, UK;* [b]*Department of Mathematics, South Kensington Campus, Imperial College London, London, UK*

(*Received 22 August 2014; accepted 2 October 2014*)

DNA nanotechnology promises to provide controllable self-assembly on the nanoscale, allowing for the design of static structures, dynamic machines and computational architectures. In this article, I review the state-of-the art of DNA nanotechnology, highlighting the need for a more detailed understanding of the key processes, both in terms of theoretical modelling and experimental characterisation. I then consider coarse-grained models of DNA, mesoscale descriptions that have the potential to provide great insight into the operation of DNA nanotechnology if they are well designed. In particular, I discuss a number of nanotechnological systems that have been studied with oxDNA, a recently developed coarse-grained model, highlighting the subtle interplay of kinetic, thermodynamic and mechanical factors that can determine behaviour. Finally, new results highlighting the importance of mechanical tension in the operation of a two-footed walker are presented, demonstrating that recovery from an unintended 'overstepped' configuration can be accelerated by three to four orders of magnitude by application of a moderate tension to the walker's track. More generally, the walker illustrates the possibility of biasing strand-displacement processes to affect the overall rate.

Keywords: DNA nanotechnology; self-assembly; molecular machines; non-equilibrium systems; coarse-grained modelling; simulation

1. Introduction to DNA nanotechnology

1.1. The DNA molecule and its potential

Deoxyribonucleic acid (DNA) is a macromolecule with a backbone of covalently linked sugar and phosphate groups; attached to each sugar is a base, which can be adenine (A), guanine (G), cytosine (C) or thymine (T) [1]. DNA is often found as a double helix of antiparallel strands stabilised by hydrogen-bonding of complementary Watson–Crick base pairs (AT and CG) and stacking interactions between the planar bases. Double-stranded DNA (dsDNA) is stiff, with a persistence length of ∼150 base pairs [2], whereas unpaired single strands (ssDNA) are far more flexible [3,4].

DNA carries information through its sequence of bases – in biology, this information codes for proteins and their regulation. The specificity of Watson–Crick base-pairing means that both strands within a duplex carry identical information, facilitating replication. In 1982, Seeman speculated that the specificity of DNA hybridisation could be harnessed to permit the design of artificial structures, proposing that certain sequences could self-assemble into crystals [5].

1.2. DNA nanostructures

The Seeman group quickly constructed artificial nucleic acid junctions [6], but the first three-dimensional crystal based purely on rationally designed Watson–Crick base pairs was not demonstrated until 2009 [7] (crystals involving non-canonical interactions were created in 2004 [8]). In the intervening period, ribbons [9] and two-dimensional lattices [10,11] were realised. Complex Archimedean tiling patterns [12] and 'empty liquids' [13] have recently been achieved through hybridisation-driven DNA self-assembly.

As well as macroscopic phases, DNA can form structures of well-defined finite size. Early successes (cubes [14] and octahedra [15]) involved several discrete stages of assembly, but it was subsequently shown that polyhedra [16–18] and then more complex structures [19,20] could be made to form simply by cooling solutions of short ssDNA strands (oligonucleotides). An alternative approach, known as DNA 'origami' [21], uses one long 'scaffold' strand that is shaped by shorter 'staple' strands into a complex structure. This technique can produce three-dimensional objects [22,23] and structures with curvature or twist [24,25]. Some examples of DNA nanostructures are shown in Figure 1(a)–(c).

DNA does not have to be used in isolation – it can also be conjugated with other molecules or nanoparticles. Crystals of DNA-coated colloids have been constructed [26], and small organic molecules have been used as vertices in structures held together by DNA [27,28].

* Email: t.ouldridge@imperial.ac.uk

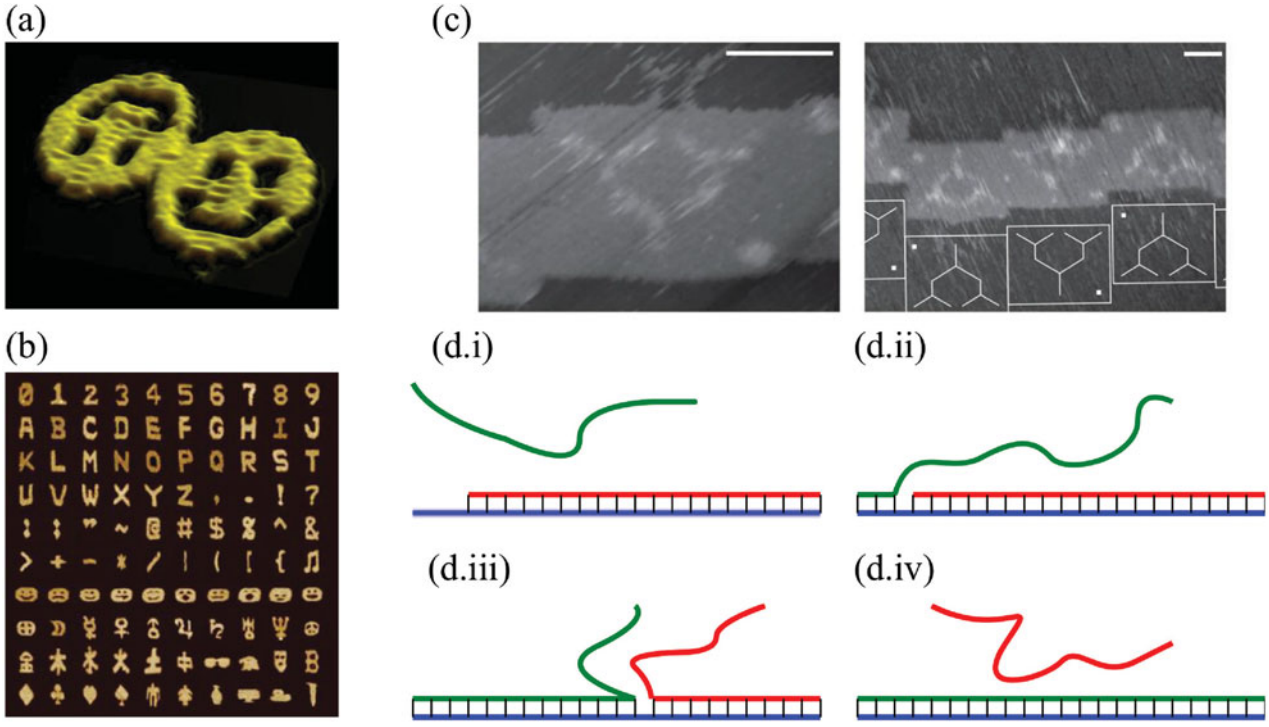

Figure 1. (a)–(c) Examples of DNA nanotechnology. (a) Atomic force microscopy (AFM) image of the original DNA 'origami' [21], courtesy of P. W. K. Rothemund. (b) AFM of complex structures assembled from DNA 'bricks' [20], courtesy of P. Yin. (c) Tracks for a DNA-based motor on origami. Reprinted by permission from Macmillan Publishers Ltd: Nature Nanotechnology [29], copyright 2012. (d) Basic displacement. (d.i) The initial state with incumbent (red) and substrate (blue) bound and the invader (green) free in solution. (d.ii) The invader binds to the available toehold of the substrate. (d.iii) The invader competes with the incumbent for base pairs. (d.iv) The final state, in which the invader has completely displaced the incumbent. (Colour online)

1.3. Dynamic DNA devices

DNA is not restricted to static nanostructures, but can be used to create dynamically active nanoscale objects. Toehold-mediated strand displacement (TMSD), illustrated in Figure 1(d), is used along with hybridisation to drive conformational changes in many such devices. TMSD involves the replacement of a strand (the incumbent) from a duplex with the substrate by an alternative strand (the invader) that is complementary to an additional toehold of the substrate. Initially, the invader can bind to the exposed toehold, as shown in Figure 1(d.ii) [30–32]. The invader and incumbent can then compete for base-pairing, as illustrated in Figure 1(d.iii). If, eventually, the incumbent loses all of its base pairs, it will detach and displacement is complete (Figure 1(d.iv)). As well as being essential in dynamic nanotechnology, displacement may occur during the assembly of complex structures that initially form unintended bonds between the wrong strands.

The simplest devices are switches that respond to a change in experimental conditions. An iconic example is the 'tweezers' of Yurke *et al.* [33], which can be closed and opened by sequential addition of 'fuel' strands (which bind to and closes the tweezers) and 'antifuel' strands (which displace the tweezers from the fuel, opening them). Switches can allow large structures to open, close or undergo topological rearrangement [23,34–36].

DNA 'walkers' couple the mechanical change generated by DNA reactions to motion along extended tracks, analogous to biological motors such as kinesin and myosin. The earliest designs used sequential strand addition to generate unidirectional motion along a series of binding sites ('stators') [37,38]. Solution conditions can also be modulated in different ways, for example through periodic exposure to light of different frequencies [39]. Autonomous motors, which do not rely on external control, must catalyse the release of free energy [40]. To meet this requirement, designs often couple motion to the hydrolysis of a nucleic acid strand that is not part of the walker itself. Hydrolysis can be achieved either with [41–43] or without [44–46] the involvement of an additional enzyme. An alternative is to catalyse DNA hybridisation itself [47,48] if the reactants are present as metastable self-bonded hairpins. Many walkers destroy the track behind them in the so-called 'burnt bridges' approach. The Turberfield group have also demonstrated the possibility of autonomous motion on a track that can be reused [42,47]. In the majority of cases, hybridisation and displacement are central to walker operation, sometimes in combination with additional enzymatic

reactions. An alternative is to use four-way branch migration rather than displacement [49,50].

A third branch of active DNA nanotechnology is computation. In 1994, Adleman showed that a Hamiltonian path problem could be solved using DNA [51]. Subsequently, researchers have developed motifs for logical operation based on TMSD [52], with Qian and Winfree having incorporated multiple gates into a decision-making 'brain' [53], and Chen *et al.* having developed a general architecture for control networks [54].

1.4. Applications of DNA nanotechnology

Many nanotechnological systems are elegant proofs of principle, rather than being directly useful. The potential of DNA nanotechnology, however, is obvious. Seeman's original motivation was to use DNA crystals to conjugate proteins and facilitate crystallography; origami bundles and two-dimensional lattices have indeed been used to aid protein structure determination [55,56]. Similarly, finite-sized nanostructures contain unique strands at well-defined locations. This allows nanostructures to function as nanoscale breadboards for biophysical systems – they have been used as backbones for plasmonic devices [57] and light-harvesting complexes [58], to control [59,60] and facilitate the study of [61–63] enzymatic reactions, and to provide tracks for DNA motors [29,64] (as shown in Figure 1(c)). DNA nanostructures have also been designed to act as microscopic gene-detecting arrays [65,66]. The freedom to design complex structures allows DNA to be used for other experimental components, including 'handles', 'frames' and 'rulers' for single-molecule manipulation [67,68], and harnesses for arrays of motor proteins [69].

The therapeutic potential of DNA nanotechnology has long been recognised. Nanostructures can encapsulate molecules either covalently or non-covalently [70,71], with the aim of selectively releasing them at the surface of or inside specific cells. Alternatively, nanostructures can coordinate biomolecules to mimic pathogens, potentially triggering stronger immune responses [72–74] and allowing the design of novel vaccines [74]. DNA computation may also prove to be most valuable in medical applications, when its enormous parallel capacity and direct interaction with biomolecules will prove most advantageous. Towards this end, both the uptake of small nanostructures into cells [72,75,76] and specific targeting of cancer cells by DNA-transported drugs [70] have been demonstrated. Large DNA nanostructures have been reported to be survive intact in cell lysate [77], and DNA-based devices and structures have been shown to be stable within *C. elegans* for hours or days, depending on the design [78]. The Shih lab has also shown that lipid encapsulation of nanostructures can help to shield them from digestion by nucleases when this is an issue [79] and coating origami with virus capsid proteins has been shown to improve transfection into cells [80]. Interacting 'robots' have even been demonstrated to perform computations based on the TMSD within a living organism [81].

Artificial walking devices could function as agents in molecular assembly lines, incorporating some degree of decision-making. Preliminary work has demonstrated that DNA hybridisation can accelerate and template reactions [82,83], that walkers can make decisions at junctions [29,50] and that walkers can selectively pick up gold nanoparticle cargo [84].

1.5. Understanding and optimising DNA nanotechnology

If DNA nanotechnology is to be widely used, assembly processes and operation cycles must be understood and optimised. Simple self-assembling structures such as DNA tetrahedra form reliably when a solution of reactants is rapidly cooled [16]. Larger systems tend to be more complex, although recent work has shown that substantial structures can form surprisingly well if the temperature is carefully chosen [85,86]. It is not obvious, however, why assembly can be so successful given previous failures with large colloidal structures [87]. It is also not clear why origami assembly can occur over a very narrow temperature window [85], with significant hysteresis [85,88]. Improving yields of larger structures by choosing sequences to minimise unintended cross-interactions has shown surprisingly little promise thus far [19,20], but origami assembly is very sensitive to the staple layout [86,89,90]. Even if an object appears to form well, some strands might be absent, possibly compromising its usefulness and mechanical properties [91]. Optimisation is even more important for dynamic nanotechnology, where relatively slow unintended reactions can compromise device operation [64]. For example, even if a walker has only a 5% chance of detaching from the track at each step, most will fail to take 20 steps. As it stands, motors are slow compared to natural analogues, and systematic approaches for improving their effectiveness or decision-making abilities are currently limited.

Recent experiments have probed specific systems relevant to nanotechnology in detail [31,64,85,86,89,90,92–94]. To interpret these results, generalise the resultant ideas and develop new principles, these systems must be modelled theoretically. To date, the main theoretical tool has been the nearest-neighbour model of DNA thermodynamics [95], implemented in online tools such as NuPack [96]. The nearest-neighbour model functions at the level of secondary structure (i.e., lists of the base-pairing that is present in the system). The free energy of a given secondary structure can be estimated by summing contributions from each neighbouring 'stack' of base pairs, plus contributions from end effects and enclosed loops. Whilst the nearest-neighbour model is extremely useful, it has several limitations. First,

it is a thermodynamic model with discrete states and hence has no natural kinetics [32]. Second, it does not explicitly represent DNA structure, and struggles to describe complex interconnections, loops and 'pseudoknots' [96] that often arise in nanotechnological systems. Finally, DNA mechanics is ignored, meaning that the effects of forces and torques cannot be directly understood.

Next, I will introduce coarse-grained models of DNA, mesoscale representations that can overcome the limitations of the nearest-neighbour description. I will focus on oxDNA, a model explicitly designed for DNA nanotechnology. I will outline the model, before discussing previous applications in understanding TMSD in a variety of contexts. Finally, new results will be presented on displacement involving a two-footed DNA walker [42], highlighting the possibility of accelerating displacement through mechanical strain.

2. Coarse-grained modelling of DNA nanotechnology

Coarse-grained models provide a level of resolution between fully atomistic treatments and secondary-structure descriptions like the nearest-neighbour model. Atomistic treatments are generally too computationally expensive for nanotechnological applications, although some structural studies have been performed [97,98]. Coarse-grained models represent individual nucleotides using a small number of interaction sites, which interact through effective potentials. If well parameterised, they can capture the known thermodynamic, structural and mechanical properties of DNA in a simple and naturally dynamical representation.

The choice of interactions determines the accuracy and applicability of the model. A 'bottom-up' approach is to fit interactions to reproduce correlation functions from more detailed atomistic simulations [99–113], or data from experimentally determined structures [100,109,114,115]. This procedure can be very effective, but it has limitations. First, the resultant model is very dependent on the source data, which are usually primarily drawn from duplex DNA, whereas nanotechnological systems involve ssDNA and hybridisation transitions (one exception has focused specifically on ssDNA only [111]). Even if a wider variety of systems were to be used for parameterisation, it is not clear whether current atomistic representations accurately describe isolated ssDNA and the hybridisation transition. Second, one cannot retain all features of a system when coarse-graining; 'representability problems' arise [116]. For a given set of coarse-grained degrees of freedom, the optimal potential for correlation functions will likely be distinct from that for thermodynamics. Related issues are relevant to potentials derived from *ab initio* calculations [117].

Representability problems highlight the fact that coarse-grained models cannot be perfect, and hence should be designed with their purpose in mind. For nanotechnological systems, models must capture ssDNA, dsDNA and their interconversion. To date, this has been most successfully done with 'top–down' approaches [118–136]. Here, physically motivated interactions such as hydrogen-bonding and stacking are included and parameterised to reproduce overall thermodynamic, mechanical and structural properties of DNA. In this article, I focus on oxDNA [137–139], an attempt to incorporate thermodynamics as parameterised by the nearest-neighbour model into a description with continuous degrees of freedom that captures structural and mechanical properties of DNA. Due to the emphasis placed on capturing the duplex formation transition in the development of oxDNA, it has been used to study nanotechnological systems more extensively than other models. However, duplex and hairpin formation transitions have been systematically investigated by a number of groups [119–121,123,124,127,131,133,140–144], nanostructure conformation has been studied by Bombelli *et al.* and Arbona *et al.* [130,145] and nanostructure assembly [146–148] and displacement [149] have been demonstrated with much simple models of DNA. Large-scale asssembly of DNA-coated objects has also been achieved with some simpler coarse-grained models [120,136,150]. It is worth noting that similar top–down [133,151–157] and bottom–up [158–161] models exist for RNA.

2.1. *oxDNA*

oxDNA treats each nucleotide as a three-dimensional rigid body. The potential energy of a configuration is given by

$$V = \sum_{\langle ij \rangle} (V_{\mathrm{b.b.}} + V_{\mathrm{stack}} + V'_{\mathrm{exc}}) + \sum_{i,j \notin \langle ij \rangle} (V_{\mathrm{HB}} + V_{\mathrm{cr.st.}} + V_{\mathrm{exc}} + V_{\mathrm{cx.st.}}) . \quad (1)$$

Here, the first sum runs over all consecutive pairs of nucleotides on a strand, and the second sum over all remaining pairs. The interactions represent hydrogen bonding (V_{HB}), cross stacking ($V_{\mathrm{cr.st.}}$), coaxial stacking ($V_{\mathrm{cx.st.}}$), nearest-neighbour stacking (V_{stack}), excluded volume (V_{exc} or V'_{exc}) and backbone chain connectivity ($V_{\mathrm{b.b.}}$). These interactions are shown schematically in Figure 2, and are discussed in detail elsewhere [137–139]. Importantly, attractive interactions depend explicitly on the relative orientations of nucleotides, allowing the anisotropic nature of bases to play a role.

Hydrogen-bonding and stacking interactions drive the formation of duplexes with helical structure from single strands that are relatively more disordered. oxDNA reproduces the thermodynamic, mechanical and structural changes associated with this transition, under high salt conditions. In particular, oxDNA provides a good

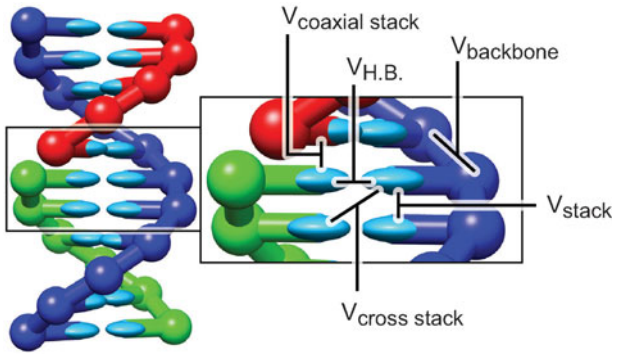

Figure 2. Illustration of the duplex structure and stabilising interactions with the oxDNA model. Spheres represent the backbone sites, and ellipsoids represent bases. Strands are coloured according to their identity. Coaxial stacking acts like a nearest-neighbour stacking interaction between bases that are not consecutive on the same strand. Excluded volume interactions (not illustrated here) also exist between all backbone and base sites. Reprinted with permission from Ouldridge *et al.* [178]. Copyright (2013) American Chemical Society. (Colour online)

representation of duplex melting temperatures, melting transitions widths, self-complementary hairpin stability, duplex elastic moduli and the short persistence length of single strands (details are provided in Refs. [137–139]). Our group uses the 'Virtual Move Monte Carlo' (VMMC) algorithm (the variant in the appendix of Ref. [162]) to calculate model thermodynamics. Dynamical properties require an additional choice of model kinetics; we use Langevin [163] and Andersen-like [164] thermostats. To improve sampling, our group has made extensive use of umbrella sampling (US) [165] for thermodynamic averages and forward flux sampling (FFS) [166,167] for kinetic studies.

Several important simplifications are inherent in the model. First, oxDNA was fitted at a salt concentration of $[Na^+] = 0.5$ M, where electrostatics is strongly screened – the repulsion of phosphates is therefore incorporated into the backbone excluded volume for simplicity. A recent study by Wang and Pettitt [168] has explored the possibility of incorporating a Debye-Hückel description of electrostatics, allowing lower salt conditions to be simulated, but the results reported in this work do not include this term. Second, model duplexes are symmetric, meaning that both grooves of the helix are of same size. Such a simplification may be of relevance when systems are extremely sensitive to geometric details; for example, the stress imposed on helices by crossovers at origami junctions will be affected by grooving. Third, as nanotechnology typically involves low concentrations of DNA, oxDNA takes the partial pressure of strands to be zero. Therefore, simulations of DNA with an implicit solvent in the canonical ensemble are appropriate for comparisons to typical experimental systems at constant temperature and pressure [169]. Consistent with this picture, we interpret free energies measured in simulations as Gibbs (rather than Helmholtz) free energies. Finally, the Langevin and Andersen-like thermostats do not incorporate collective hydrodynamic motion, and low friction coefficients are typically used to accelerate dynamics. Given these and other simplifications, it is important to identify the underlying cause of any phenomena observed in simulation, to ensure that they arise from real DNA physics rather than artefacts of the model or dynamical algorithm.

3. Insights into strand displacement from oxDNA

I now outline how oxDNA has been used to understand basic TMSD, and then to explore variants relevant to nanotechnology.

3.1. *Basic displacement*

TMSD was experimentally characterised by Zhang and Winfree [31]. These authors demonstrated that for short toeholds, displacement rate increases exponentially with toehold length, before plateauing in the long toehold limit. The results, a subset of which are reproduced in Figure 3(a), show that displacement accelerates by a factor of $\sim 10^{6.5}$ as the toehold is increased from 0 to 15 base pairs (for a displacement domain of 20 base pairs, at 25 °C and with a high salt concentration of $[Mg^{2+}] \approx 10$ mM). The overall shape of the graph is unsurprising. At the low strand concentrations used in Ref. [31], the three-stranded intermediate (including states depicted in Figure 4(a.ii), 4(a.iv) and 4(b)) is short-lived and the reaction is effectively second order. In this limit, the reaction rate constant can be modelled as

$$k_{\mathrm{eff}} = k_{\mathrm{bind}} P_{\mathrm{suc}}, \tag{2}$$

where k_{bind} is a toehold binding rate constant and P_{suc} is the probability that displacement succeeds (as opposed to the invader detaching) once the toehold is formed. For very short toeholds, it is reasonable that $P_{\mathrm{suc}} \ll 1$. Increasing the toehold length increases the toehold stability, and hence P_{suc}, exponentially. Eventually this increase with toehold length saturates when $P_{\mathrm{suc}} \sim 1$. Given that k_{bind} would be expected to be relatively weakly length dependent, k_{eff} therefore plateaus at this point.

A simple argument, however, would suggest that a single-base toehold should have a success rate greater than 1%, thereby limiting the possibilities for increasing k_{eff} by increasing the toehold length and hence P_{suc}. Consider the system illustrated in Figure 4(a), with a toehold of one base, and assume that displacement is a random walk in which base pairs at the junction can break and then be replaced by base pairs with the competing strand, as shown in Figure 4(a). From the toehold-bound state, two things can happen – either the toehold detaches, or the first base pair in the incumbent/substrate breaks. If the latter, the invader subsequently takes a base pair from the incumbent with probability 0.5, otherwise the system returns to the initial

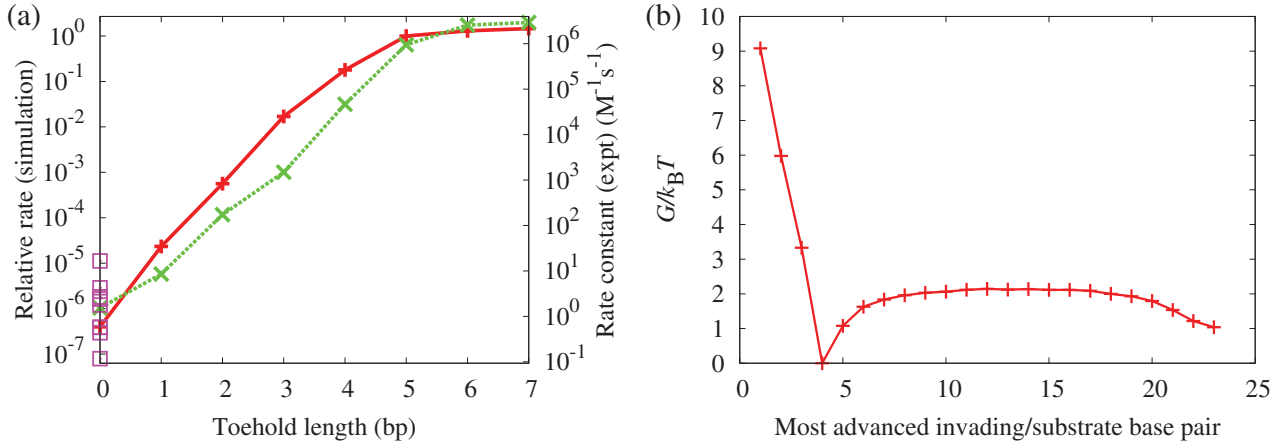

Figure 3. (a) Experimentally measured rate constants as a function of length for an average-strength toehold [31] (green 'x' symbols), compared to the relative displacement rates found for oxDNA (red '+' symbols, reported relative to the five base-pair case) [32]. Purple squares show the new estimates of zero-toehold displacement rate for oxDNA presented in this work (detailed in the Supplemental data), showing substantial measurement uncertainty. Although not quantified here, this uncertainty is much smaller for longer toeholds, when the process is easier to sample [32]. The minor variation between rates for long toeholds demonstrates the small error in this limit. (b) Free energy (G) profile of displacement in oxDNA as a function of the most advanced invader/substrate base pair for a four-base toehold. Base pair '1' is at the far end of the toehold from the displacement domain, and base pair 4 is immediately adjacent to the displacement domain [32]. Typical errors on these measurements are smaller than the '+' symbols, as estimated through comparison of independent simulations [32]. (Colour online)

state. If toehold detachment (involving the disruption of a single base pair), and breaking of base pairs at the junction have similar rates, the probability that the invader manages to take the first step is then approximately 1/3. From here, 19 more displacement steps are required, whereas the initial state is one backwards step away. From the statistics of random walks, we obtain $P_{\mathrm{suc}} \sim \frac{1}{3}\frac{1}{20} \sim 0.02$ for single-base toeholds. Given this estimated value of P_{suc} for a single-base toehold, it is difficult to justify the extent of the experimentally observed slowdown for shorter toeholds.

The displacement process has been simulated with oxDNA, as outlined in Ref. [32]. The results shown in Figure 3(a) agree well with those obtained by Zhang and Winfree [31]. The key point, however, is not the quality of agreement, but that oxDNA also violates the simple argument outlined above which suggests only a modest slowdown for short toeholds. By studying oxDNA, we can then hope to explain the experimental results. Explanations for this behaviour, violations of two assumptions of our simple argument, are given discussed in detail Ref. [32].

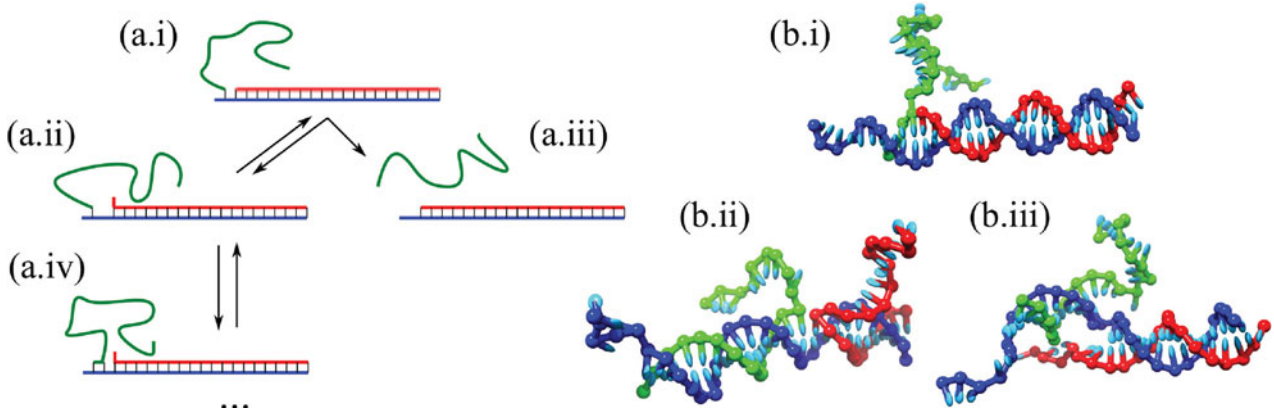

Figure 4. Representations of displacement at two levels in detail. In both cases, the substrate is blue, the invader green and the incumbent red. (a) Illustration of a simple step-by-step model of displacement for a one-base toehold. Starting from the toehold-bound state (a.i), either a base pair between incumbent and substrate can break (a.ii) or the toehold base pair can break, leading to detachment (a.iii). From state (a.ii), either the invader can bind to the newly revealed substrate base (a.iv), or the incumbent can rebind, returning us to the initial state (a.i). This process can be repeated for every base in the displacement domain. (b) Displacement in oxDNA (for a three-base toehold). (b.i) The toehold-bound state. (b.ii) A later stage of displacement. (b.iii) A later stage of displacement in which the invader and incumbent duplexes have unstacked at the displacement junction. (Colour online)

First, junction migration is not an unbiased random walk. As junction migration is initiated, a second single-stranded section is generated at the displacement junction, as can be seen in Figure 4(b). This second overhang is thermodynamically unfavourable, due to steric exclusions at the junction, and consequently biases the system against initiating and proceeding with junction migration. It therefore reduces the probability of successful displacement given toehold binding. A free-energy profile indicating a thermodynamic cost for initiating displacement is shown in Figure 3(b) (the free energy as a function of an order parameter, $G(Q)$, is a measure of the probability that the system exists in state Q, $P(Q)$: $G(Q) = -k_{\mathrm{B}}T \ln P(Q) + \text{const}$).

Second, simulations show that junction migration is far more complex than the breaking of a single base pair in the toehold, necessarily involving the disruption of more stacking interactions and a greater structural rearrangement. Junction migration is then intrinsically slow compared to the disruption of toehold base pairs, again reducing the probability of displacement as opposed to detaching from the toehold.

Winfree and co-workers have used the thermodynamic stability of 'frozen' displacement intermediates to explore the possibility of the penalty associated with dangling ss-DNA at the junction, confirming its existence and estimating a value of $\sim 3k_{\mathrm{B}}T$, slightly larger than found for oxDNA [32]. Analysis of a simple secondary-structure based model [32] suggests that such an impediment provides only a partial explanation of the degree to which longer toeholds can accelerate displacement. As a consequence, the second factor identified by oxDNA as inhibiting displacement (slow junction migration) seems necessary to explain the wide range of rates as a function of toehold length.

3.2. *Displacement involving mismatches*

The plateau in displacement rate as toehold length increases limits the maximal selectivity for intended processes over leak reactions. Modifying displacement to reduce its success probability would enlarge the regime in which rate grows with toehold stability, and hence the dynamic range and maximal selectivity. Authors have included physical separation of the toehold from the displacement domain [171] or forced the invading strand to create unfavourable 'mismatched' base pairs [172,173] to achieve this. The principle is generally to slow displacement by decreasing the overall free-energy gain $|\Delta G^{\mathrm{disp}}|$ of the reaction.

OxDNA has been used to simulate displacement in which a C–G base pair is replaced by a C–C mismatch as displacement proceeds [170]. Mismatches were considered at the start, in the middle and 4 base pairs from the end of a 16-base displacement domain, for a toehold of 5 bases. In each case, the mismatch destabilises the final invader/substrate duplex by approximately $\Delta\Delta G^{\mathrm{disp}}_{\mathrm{mm}} = 5.9k_{\mathrm{B}}T$. We might then naïvely expect a rate reduction by a factor

$$\frac{k^{\mathrm{mm}}_{\mathrm{eff}}}{k^{\mathrm{perfect}}_{\mathrm{eff}}} \approx \exp\left(-\Delta\Delta G^{\mathrm{disp}}_{mm}/k_{\mathrm{B}}T\right) \approx \frac{1}{350}. \qquad (3)$$

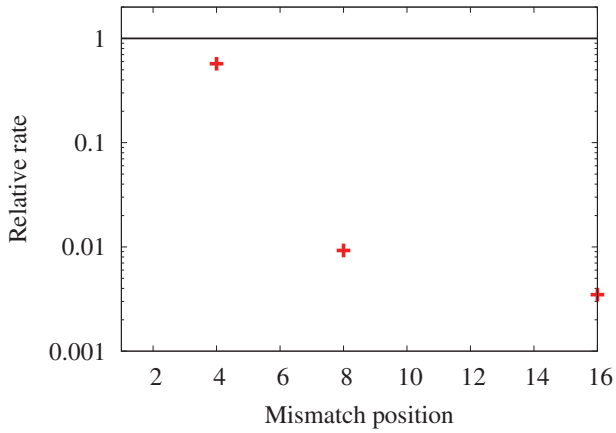

Figure 5. Relative rates of displacement as a function of the position of a mismatch created during displacement (as predicted by oxDNA) [170]. The position is defined with respect to the far end of the displacement domain (which has a length of 16 base pairs in this system) – a mismatch at position '16' is immediately adjacent to the toehold, and a mismatch at position '4' is near the far end of the displacement domain. Values are reported relative to the rate for a perfectly matched invader, and the all points are estimated to have an error less than or equal to a factor of two, as estimated through independent simulations [170]. (Colour online)

The results, taken from Ref. [170] and shown in Figure 5, are initially surprising. The early mismatch does indeed cause a slowdown by $\sim$350, and the middle mismatch by a factor $\sim$100. The late mismatch, however, has almost no influence. This result must mean that P_{suc} is high despite the late mismatch. The fact that the mismatch is far from the toehold certainly helps – after encountering the mismatch, the junction must migrate 12 steps backwards before the invader is bound only to the toehold, raising the probability that displacement will occur anyway despite the impediment. However, mismatches are so destabilising ($5.9k_{\mathrm{B}}T$ in this case) that it is still difficult to see how enclosing it and subsequently completing junction migration would not be slow compared to returning to the toehold-only state. The resolution of this paradox is the existence of an alternative pathway, in which the incumbent strand spontaneously detaches from the substrate at a stage when the invader has not yet enclosed the mismatch. This pathway should be contrasted with the standard picture of base-by-base displacement [32]. The invader/substrate base pairs beyond the mismatch are then formed at a later stage, when there is no competition from the incumbent, and the full penalty of $\Delta\Delta G^{\mathrm{disp}}_{\mathrm{mm}}$ is not manifest in the displacement reaction rate. This alternative pathway is illustrated schematically,

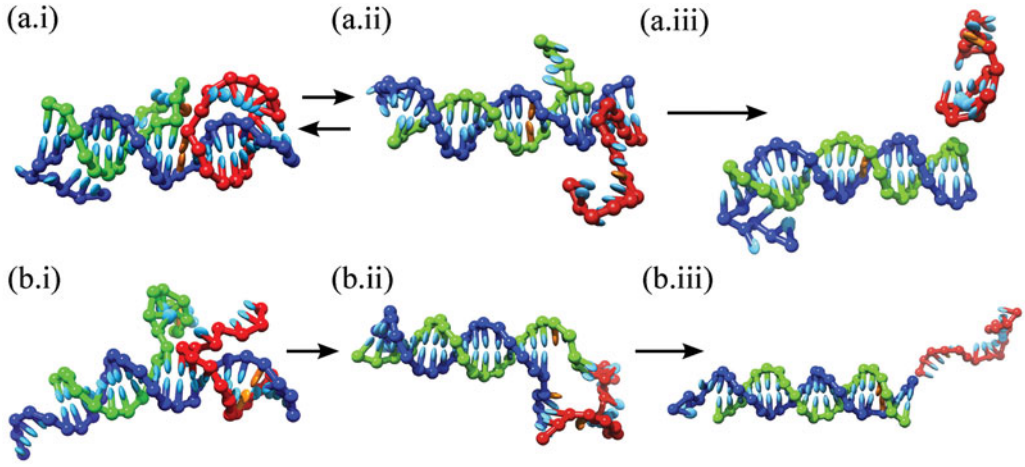

Figure 6. Distinct pathways for displacement involving the creation of a mismatched base pair. The incumbent is shown in red, the invader in green and the substrate in blue. The location of the mismatch is highlighted by the orange-coloured bases. (a) Creating a mismatch in the middle of the displacement domain. The typical pathway involves enclosure of the mismatch (a.ii) prior to detachment of the incumbent and the completion of displacement (a.iii). (b) Creating a mismatch four bases from the end of the displacement domain typically involves detachment of the incumbent (b.ii) prior to enclosure of the mismatch (b.iii).

and contrasted with a displacement pathway which involves enclosing the mismatch, in Figure 6.

Spontaneous detachment involves breaking a number of base pairs. When the mismatch is late in the displacement domain, it is feasible for the incumbent to detach spontaneously when the invader reaches the mismatch location. This process is somewhat analogous to the detachment of a short toehold, as discussed in Section 3.1. As highlighted in Section 3.1, toehold detachment is relatively fast compared to completing displacement; this explains why spontaneous detachment involving the disruption of several base pairs can be a kinetically favoured pathway, even when the most stable final state involves enclosure of the mismatch by the invader/substrate duplex.

As the mismatch is moved towards the start of the displacement domain, the number of base pairs that must break spontaneously grows and the rate of detaching in this way is exponentially suppressed. Eventually, spontaneous detachment is so slow that it is no longer faster than simply continuing displacement in the conventional base-by-base manner, and enclosing the mismatch. For oxDNA, both the middle and early mismatches are in this regime and hence they feel the effect of $\Delta\Delta G^{\mathrm{disp}}_{\mathrm{mm}}$. The difference between middle and early mismatches arises not from differences in the rate at which displacement occurs given toehold binding, but actually due to slower toehold detachment for the middle mismatch [170].

In general, oxDNA predicts that mismatches formed at the start of a displacement domain will heavily suppress displacement rates. Rates should initially rise slightly as the mismatch is moved towards the far end of the domain (away from the toehold). At some point, the spontaneous melting pathway will become relevant and the overall rate will rise rapidly, eventually plateauing at the perfectly matched value. Recent experiments have demonstrated exactly this behaviour [170], showing that oxDNA is a powerful tool for probing DNA reaction dynamics.

These results emphasise that mismatches should be placed at the start of the displacement domain to slow displacement and thus suppress the rate of leak reactions. Recent work has considered using displacement to resolve single-nucleotide polymorphisms in genes [66,174–176]; oxDNA suggests that the simplest kinetic methods might struggle to detect mutations at the end of a displacement domain [66,174], although modified approaches might far better [175,176]. More generally, the results illustrate a mechanism for modulating reaction kinetics by orders of magnitude whilst maintaining approximately the same overall reaction thermodynamics. A corollary is that reverse reactions will be far faster for the late mismatch, which may also be important when designing nanotechnological systems.

3.3. *Displacement during the cycle of a burnt-bridges motor*

OxDNA has been used [177] to model a burnt-bridges DNA motor designed by Turberfield and co-workers [29,41,43]. The motor is illustrated in Figure 7(a). I will focus on the mechanism by which the motor strand (or 'cargo') steps from one stator (a single-stranded binding site anchored to the track) to the next via displacement – a simulation snapshot of this process is shown in Figure 7(b). The free-energy profiles of displacement, for various distances d_s between the stators, are shown in Figure 8. As d_s is increased, toehold formation becomes slightly less favourable, due to a greater loss of entropy associated with toehold binding when the

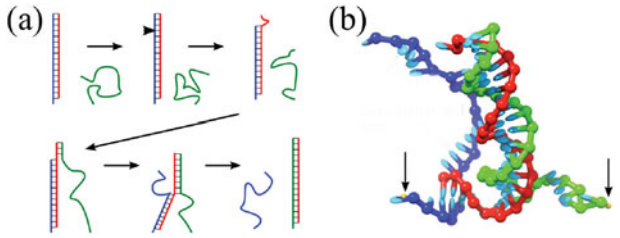

Figure 7. The burnt-bridges motor introduced in Ref. [41]. (a) A schematic of motor operation. The cargo (red) is initially bound to the first stator (blue). A nicking enzyme cuts this stator, revealing a toehold (six bases in this case) for an alternative stator (green) which can displace the original, resulting in a step of the cargo strand. (b) An intermediate stage of stepping as represented by oxDNA. The two stators are anchored at points indicated by the vertical arrows. From this figure, it is clear that the final stages of displacement involve subjecting the motor to considerable tension as it stretches between the two anchoring points. (Colour online)

stators are further apart. Far more significant, however, is the rise in free energy at later stages that can be seen for large d_s. As displacement progresses, fewer bases are available to stretch across the gap between the points at which the stators are anchored, as shown in Figure 7(b). Displacement must then work against the tension of these stretched bases, meaning that the free energy rises as displacement progresses.

Some caution must be exercised when using free-energy profiles to infer kinetics. If the low-dimensional order parameter used is not a perfect reaction coordinate, signatures of kinetic effects may be hidden. Indeed, the relative difficulty of junction migration highlighted in Section 3.1 is not easily identified in free-energy profiles at the level of base pairs. Nonetheless, large stator separation will clearly

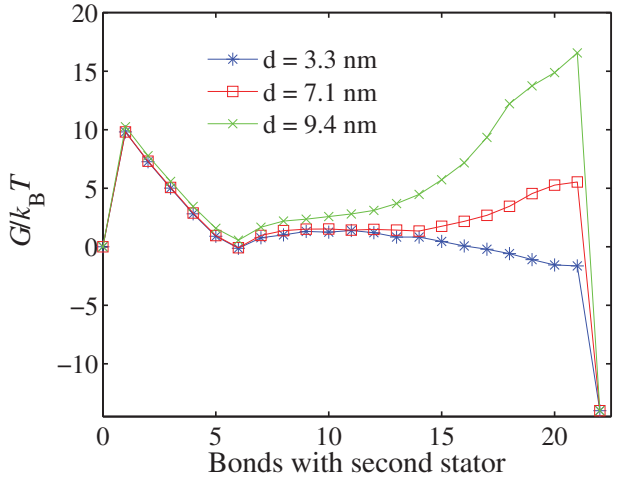

Figure 8. Free-energy (G) profiles as a function of the number of bonds with the second stator during the displacement stage of the cycle of a burnt-bridges motor. Profiles are shown for three different separations between the anchoring points of the stators. Reprinted with permission from P. Šulc *et al.* [177]. Copyright (2013) Springer Science and Business Media. (Colour online)

frustrate motor stepping, primarily due to lower rates of displacement once the toehold is formed, rather than slow toehold formation. Moderately large stator separations could then be used like early mismatches to reduce displacement success probabilities, thereby increasing the toehold length required to saturate P_{suc} at unity and suppressing leak reactions relative to the rate in this long-toehold limit. This approach would be particularly useful at junctions where decisions must be made [29]. If d_s primarily influenced binding rates, rather than success probabilities, larger d_s would not help to discriminate between toeholds but would slow all reactions equally.

It is worth noting that slowing displacement by increasing d_s alters reaction kinetics without changing the overall ΔG of reaction. This is similar to changing the location of a mismatch formed between invader and substrate, but unlike increasing the number of mismatches. This is because the initial and final states, in which the cargo is bound to one stator only, are not d_s-dependent. Large values of d_s can in principle be used at an arbitrarily large number of stages for the same cargo molecule without destabilising the final product. This advantage of modulating kinetics with d_s must be weighed against the fact that the motif is limited to sequential reactions on a surface.

4. Recovery of a two-footed walker: an example of enhanced displacement

Turberfield and co-workers have also introduced a two-footed DNA walker that is designed to achieve directional motion without modifying its track, a continuous single strand consisting of multiple binding sites [42]. The walker is intended to step in a foot-over-foot fashion; its full design is given in Ref. [42]. It is intended to exist either with a single foot bound to the track and the other raised, or with both feet bound to overlapping adjacent sites, as illustrated in Figure 9(a) and 9(b). The feet must overlap, as competition means that one or other of the feet will then have a raised toehold domain. A single-stranded fuel can bind to this raised domain, initiating displacement of the track and raising the foot. The fuel is designed to selectively raise the 'back' foot due to asymmetry within the system.

An earlier oxDNA study [178] revealed that the walker had a tendency to 'overstep', or bind to two non-adjacent sites (Figure 9(c)). This is disastrous for the walker, leaving both feet bound to the track without a free toehold to initiate foot lifting. This tendency was observed even with tracks under moderate tension (∼15 pN). Although tension could not prevent overstepping, increased disruption (fraying) of the front foot/track duplex hinted that recovery might be easier in the presence of tension, due to destabilisation of the overstepped state.

I now present evidence that tension does facilitate recovery from the overstepped state. I simulate toehold-free (blunt-ended) displacement of the track from the

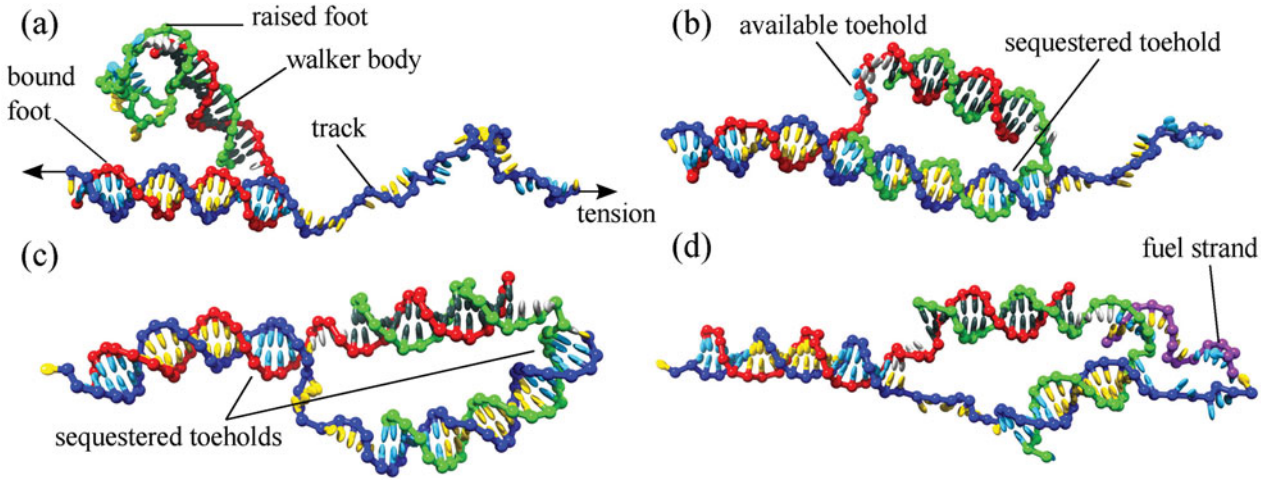

Figure 9. States relevant to the operation of a two-footed DNA walker. The backbone of the track is coloured blue, the two feet red and green and the fuel purple. Bases are coloured according to their 'domain' – sky blue bases are toehold sequences, and yellow bases constitute the longer binding domains between track and foot. Dark green bases form the duplex that holds the two feet together. The system has an inherent asymmetry which allows the definition of forward and backward directions [178]; in this figure, the forward direction is to the right. (a) Walker with one foot bound to the back site of a three-site track. (b) Walker bound to two adjacent sites on a three-site track, revealing a toehold for the fuel to raise the back foot. (c) Overstepped walker with sequestered toeholds. (d) Fuel displacing the track from the foot, prior to recovery of the walker from the overstepped state. In all figures, the track is subject to a tension of 14.6 pN in the horizontal direction.

overstepped foot by a fuel molecule, as illustrated in Figure 9(d), both with and without a tension of 14.6 pN applied to the track. Langevin dynamics simulations enhanced by FFS are used to estimate relative rates, and free-energy profiles of displacement are estimated using VMMC aided by US. Full methodological details are provided in the Supplemental data. Kinetic simulations indicate that displacement is $\sim 5 \times 10^3$ faster with tension than without, and the free-energy profiles (Figure 10) show that a difference of about $\Delta\Delta G_{\text{tension}} \approx 6.4\ k_{\text{B}}T$ develops between the two systems as displacement progresses.

When bound to two non-adjacent sites as in Figure 9(c), the walker tends to constrain the track and reduce its possible extension. Importantly, as individual base pairs between the forward edge of the front foot and the track are disrupted, the track is able to extend incrementally further (see Figure 9(d)). As a consequence, these base pairs break more easily than without tension – they have a higher tendency to be frayed prior to fuel binding, providing an effective toehold for displacement. Furthermore, because base pairs with the fuel are more stable than with the track, displacement of the track is biased towards success (as evidenced by the slope at the start of displacement in Figure 10 for the system under tension). Detailed inspection of the FFS results indicates that faster displacement is due to both easier binding and a higher subsequent probability of displacement success. If the thermodynamic results were used to estimate relative rates via $\exp(-\Delta\Delta G_{\text{tension}}/k_{\text{B}}T)$, a value of approximately 600 would be obtained. The statistical errors associated with the kinetic estimates in particular are substantial, so it is possible that the difference is due to random error. However, it is also possible that the free-energy profile fails to highlight subtle kinetic effects, such as those that were observed in conventional displacement.

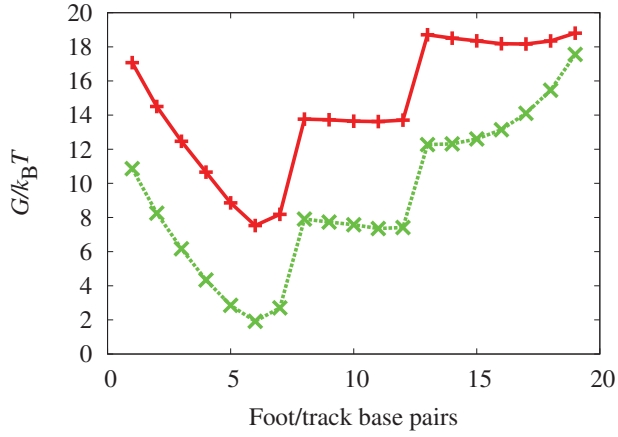

Figure 10. Free-energy profile G for the raising of the front foot of an overstepped walker, given at least one base pair between an invading fuel strand and the foot. Data are shown for systems both with (green 'x' symbols) and without (red '+' symbols) a tension of 14.6 pN applied the track. Free energies are measured relative to a reference state in which the fuel is yet to bind. Increasing displacement corresponds to reduced numbers of base pairs between foot and track – i.e., moving from right to left on the graph. Large jumps at 7–8 and 12–13 are due to the repairing of mismatches by the invader; these mismatches are present by design to prevent enzymatic cleavage of the track. Statistical errors are similar in magnitude to the size of symbols; a more detailed discussion is given in the Supplemental data. (Colour online)

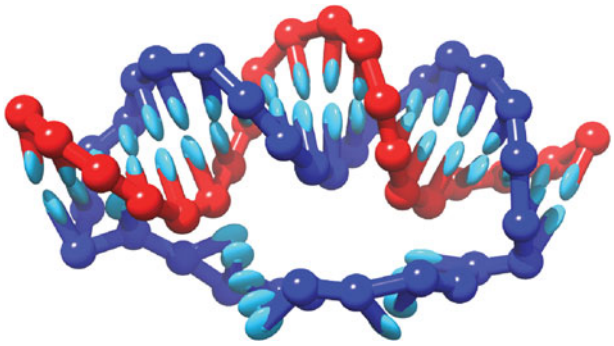

Figure 11. Generating tension that will favour displacement in a 'self-contained' manner by using a short circular strand as the incumbent. (Colour online)

Regardless, the two results clearly predict a substantial increase in walker recovery rate of $\sim 10^3$ or more under the application of moderate tension.

The fact that tension can aid walker recovery highlights the possibility of building contingency into nanodevice operation, thereby allowing for fail-safe behaviour. It also demonstrates the possibility of enhancing displacement through tension, an alternative way to modulate kinetics. In this case, tension is externally applied to the track; one possibility is to stretch the track between two points of an origami structure. One could generate tension in a more self-contained way by using circular substrates, as shown in Figure 11; indeed, similar constructs have been studied experimentally [179,180]. Here, a sufficiently long duplex section will apply an extensional stress to a sufficiently short single-stranded section, and will experience a compression in response, leading to the bending shown in Figure 11. Displacement rates in such a system could be modulated by a secondary structure within, or binding to, the single-stranded loop of the substrate – this modulation would be freed from any constraints of the invader sequence.

5. Discussion

DNA nanotechnology has enormous potential, but providing a solid theoretical underpinning is vital if it is to truly flourish. This understanding can be achieved through a combination of careful experimentation and modelling. Certain groups are now taking up the challenge of meticulously understanding the processes involved by carefully measuring important reactions in a variety of contexts [31,64,85,86,89,90,92,93]. In this article, I have discussed a coarse-grained model of DNA, oxDNA, that can complement these efforts. oxDNA is an attempt to incorporate the thermodynamics of DNA as parameterised by SantaLucia's nearest-neighbour model into a structural and mechanical framework consistent with current knowledge. It can then be used to study the behaviour of 'ideal' DNA, exploring the possibilities of certain motifs, testing whether new experimental observations are consistent with current understanding and revealing which properties of DNA have an influence on certain phenomena.

I have reviewed a number of applications of oxDNA, demonstrating that it provides quantitative understanding of aspects of displacement processes and can offer qualitative insight into reaction mechanisms and novel motifs. In each case, a physically reasonable underlying cause for the observation in question was identified, such as stress that is generated or relieved during displacement. These effects should therefore be manifest in real DNA, rather than simply being artefacts the model or simulation technique. Intriguing questions remain open, as there are many possible motifs available for study. For example, displacement reactions have recently been reported in the context of unconventional left-handed super-helices formed by conventional B-DNA domains in a complex pseudoknotted structure [181] – such a system would an ideal candidate for study with oxDNA. Other possibilities include studying the influence of single-stranded hairpins, which are frequently present both by accident and design, on hybridisation and displacement kinetics and considering general properties of displacement cascades on surfaces [94].

oxDNA's strengths are its efficiency and good overall representation of the structural, mechanical and thermodynamic changes associated with short duplex formation. To achieve efficiency, however, the description of nucleotides is extremely simple and electrostatics in particular is treated in a basic fashion. Some properties, such as the opening of internal denaturation bubbles and the structures of systems that are more complex than simple duplexes, are yet to be fully tested against experimental data. Characterising and improving these limitations will be the subject of further work.

oxDNA is parameterised to experimental data on the basic properties of DNA, but experimental results are not unequivocal. In particular, the typical state, stacking propensity and conformation of single strands are poorly understood (as discussed in Refs. [137,138]), with some authors even finding evidence for structure formation when none would be expected from Watson–Crick base pairing [182]. Single strands have an enormous role in nanotechnological systems, not least as the initial state of the hybridisation process, which itself is not unambiguously understood. Particularly pertinent open questions relate to the temperature-dependence of hybridisation, as discussed in Ref. [183], and its behaviour near a surface [92]. Mechanical properties of duplexes, and whether DNA can be described as a wormlike-chain at short length scales, are still the subject of debate [184–187]. Resolving these fundamental issues would be extremely useful in nanotechnology and beyond. It is likely that, as further characterisation is performed, some of the assumptions inherent in the current understanding of DNA (and hence oxDNA) will have to be revisited.

In this article, I have focused on the application of oxDNA to small, active systems. oxDNA has also been used to study DNA in a range of other contexts, including large duplexes under applied stress [188], and self-assembly driven phase transitions [189,190]. A modified version parameterised to describe RNA has recently been developed [191]. Although some progress has been made with improving the experimental protocols for constructing large structures [85,86,89,90], the assembly pathways and systematic ways to optimise them remain elusive. Modelling the assembly of larger structures with oxDNA is a current goal, but remains extremely challenging due to the large number of rare-event binding processes that must be observed. Further development and refinement of enhanced dynamic sampling techniques, such as FFS, would assist in this process. It may be that oxDNA can best be used to study smaller sub-structures, and that this information can then be incorporated into models at the level of secondary structure [96,192] or whole binding domains [87,88,193].

Acknowledgements

The author would like to thank J. P. K. Doye, A. A. Louis, P. Šulc, F. Romano, R. R. F. Machinek, J. Bath and A. J. Turberfield for helpful discussions. This work was funded by University College, Oxford.

Supplemental data

Supplemental data for this article can be accessed here.

References

[1] W. Saenger, *Principles of Nucleic Acid Structure* (Springer-Verlag, New York, 1984).
[2] P.J. Hagerman, Annu. Rev. Biophys. Biophys. Chem. **17**, 265 (1988).
[3] J.B. Mills, E. Vacano, and P.J. Hagerman, J. Mol. Biol. **285**, 245 (1999).
[4] M.C. Murphy, I. Rasnik, W. Chang, T.M. Lohman, and T. Ha, Biophys. J. **86**, 2530 (2004).
[5] N.C. Seeman, J. Theor. Biol. **99**, 237 (1982).
[6] N.R. Kallenbach, R.I. Ma, and N.C. Seeman, Nature **305**, 829 (1983).
[7] J. Zheng, J.J. Birktoft, Y. Chen, T. Wang, R. Sha, P.E. Constantinou, S.L. Ginell, C. Mao, and N.C. Seeman, Nature **461**, 74 (2009).
[8] P.J. Paukstelis, J. Nowakowski, J.J. Birktoft, and N.C. Seeman, Chem. Biol. **11**, 1119 (2004).
[9] H. Yan, S. Park, G. Finkelstein, J.H. Reif, and T.H. LaBean, Science **301**, 1882 (2003).
[10] E. Winfree, F.R. Liu, L.A. Wenzler, and N.C. Seeman, Nature **394**, 539 (1998).
[11] J. Malo, J.C. Mitchell, C. Venien-Bryan, J.R. Harris, H. Wille, D.J. Sherrat, and A.J. Turberfield, Angew. Chem. Int. Ed. **44**, 3057 (2005).
[12] F. Zhang, Y. Liu, and H. Yan, J. Am. Chem. Soc. **135**, 7458 (2013).
[13] S. Biffi, R. Cerbino, F. Bomboi, E.M. Paraboschi, R. Asselta, F. Sciortino, and T. Bellini, Proc. Natl. Acad. Sci. U.S.A. **110**, 15633 (2013).
[14] J. Chen and N.C. Seeman, Nature **350**, 631 (1991).
[15] Y. Zhang and N.C. Seeman, J. Am. Chem. Soc. **116**, 1661 (1994).
[16] R.P. Goodman, I.A.T. Sharp, C.F. Tardin, C.M. Erben, R.M. Berry, C.F. Schmidt, and A.J. Turberfield, Science **310**, 1661 (2005).
[17] C.M. Erben, R.P. Goodman, and A.J. Turberfield, J. Am. Chem. Soc. **129**, 6992 (2007).
[18] F.F. Andersen, B. Knudsen, C.L.P. Oliveira, R.F. Frohlich, D. Kruger, J. Bungert, M. Agbandje-McKenna, R. McKenna, J. Sissel, C. Veigaard, J. Koch, J.L. Rubinstein, B. Guldbrandtsen, M.S. Hede, G. Karlsson, A.H. Andersen, J.S. Pedersen, and B.R. Knudsen, Nucl. Acids Res. **36**, 1113 (2008).
[19] B. Wei, M. Dai, and P. Yin, Nature **485**, 623 (2012).
[20] Y. Ke, L.L. Ong, W.M. Shih, and P. Yin, Science **338**, 1177 (2012).
[21] P.W.K. Rothemund, Nature **440**, 297 (2006).
[22] S.M. Douglas, H. Dietz, T. Liedl, B. Högberg, F. Graf, and W.M. Shih, Nature **459**, 414 (2009).
[23] E.S. Andersen, M. Dong, M.M. Nielsen, K. Jahn, R. Subramani, W. Mamdouh, M.M. Golas, B. Sander, H. Stark, C.L.P. Oliveira, J.S. Pedersen, V. Birkedal, F. Besenbacher, K.V. Gothelf, and J. Kjems, Nature **459**, 73 (2009).
[24] H. Dietz, S.M. Douglas, and W.M. Shih, Science **325**, 725 (2009).
[25] D. Han, S. Pal, J. Nangreave, Z. Deng, Y. Liu, and H. Yan, Science **332**, 342 (2011).
[26] S.Y. Park, A.K.R. Lytton-Jean, B. Lee, S. Weigand, G.C. Schatz, and C.A. Mirkin, Nature **451**, 553 (2008).
[27] F.A. Aldaye and H.F. Sleiman, J. Am. Chem. Soc. **129**, 13376 (2007).
[28] J. Zimmermann, M.P. Cebulla, S. Monninghoff, and G. von Kiedrowski, Angew. Chem. Int. Ed. **47**, 3626 (2008).
[29] S.F.J. Wickham, J. Bath, Y. Katsuda, M. Endo, K. Hidaka, H. Sugiyama, and A.J. Turberfield, Nat. Nanotechnol. **7**, 169 (2012).
[30] B. Yurke and A. Mills, Genet. Program. Evolvable Mach. **4**, 111 (2003).
[31] D. Zhang and E. Winfree, J. Am. Chem. Soc. **131**, 17303 (2009).
[32] N. Srinivas, T.E. Ouldridge, P. Šulc, J. Schaeffer, B. Yurke, A.A. Louis, J.P.K. Doye, and E. Winfree, Nucl. Acids Res. **41**, 10641 (2013).
[33] B. Yurke, A.J. Turberfield, A.P. Mills, F.C. Simmel, and J. Neumann, Nature **406**, 605 (2000).
[34] H. Yan, X.P. Zhang, Z.Y. Shen, and N.C. Seeman, Nature **415**, 62 (2002).
[35] R.P. Goodman, M. Heilemann, S. Doose, C.M. Erben, A.N. Kapanidis, and A.J. Turberfield, Nat. Nanotechnol. **3**, 93 (2008).
[36] D. Han, S. Pal, Y. Liu, and H. Yan, Nat. Nanotechnol. **5**, 712 (2010).
[37] W.B. Sherman and N.C. Seeman, Nano Lett. **4**, 1203 (2004).
[38] J.S. Shin and N.A. Pierce, J. Am. Chem. Soc. **126**, 10834 (2004).
[39] M. Liu, R. Hou, J. Cheng, I.Y. Loh, S. Sreelatha, J.N. Tey, J. Wei, and Z. Wang, ACS Nano **8**, 1792 (2014).
[40] J. Bath and A.J. Turberfield, Nat. Nanotechnol. **2**, 275 (2007).
[41] J. Bath, S.J. Green, and A.J. Turberfield, Angew. Chem. Int. Ed. **117**, 4432 (2005).
[42] J. Bath, S.J. Green, K.E. Allan, and A.J. Turberfield, Small **5**, 1513 (2009).

[43] S.F.J. Wickham, M. Endo, Y. Katsuda, K. Hidaka, J. Bath, H. Sugiyama, and A.J. Turberfield, Nat. Nanotechnol. **6**, 166 (2011).

[44] Y. Tian, Y. He, Y. Chen, P. Yin, and C. Mao, Angew. Chem. Int. Ed. **44**, 4355 (2005).

[45] K. Lund, A.J. Manzo, N. Dabby, N. Michelotti, A. Johnson-Buck, J. Nangreave, S. Taylor, R. Pei, M.N. Stojanovic, N.G. Walter, E. Winfree, and H. Yan, Nature **465**, 206 (2010).

[46] T.G. Cha, J. Pan , H. Chen, J. Salgado, X. Li, C. Mao, and J.H. Choi, Nat. Nanotechnol. **9**, 39 (2014).

[47] S.J. Green, J. Bath, and A.J. Turberfield, Phys. Rev. Lett. **101**, 238101 (2008).

[48] T. Omabegho, R. Sha, and N.C. Seeman, Science **324**, 67 (2009).

[49] S. Venkataraman, R.M. Dirks, P.W.K. Rothemund, E. Winfree, and N.A. Pierce, Nat. Nanotechnol. **2**, 490 (2007).

[50] R.A. Muscat, J. Bath, and A.J. Turberfield, Nano Lett. **11**, 982 (2011).

[51] L.M. Adleman, Science **266**, 1021 (1994).

[52] G. Seelig, D. Soloveichik, D.Y. Zhang, and E. Winfree, Science **314**, 1585 (2006).

[53] L. Qian and E. Winfree, Science **332**, 1196 (2011).

[54] Y.J. Chen, N. Dalchau, N. Srinivas, A. Phillips, L. Cardelli, D. Solveichik, and G. Seelig, Nat. Nanotechnol. **8**, 755 (2013).

[55] M.J. Berardi, W.M. Shih, S.C. Harrison, and J.J. Chou, Nature **476**, 109 (2011).

[56] D.N. Selmi, R.J. Adamson, H. Attrill, A.D. Goddard, A. Watts, and A.J. Turberfield, Nano Lett. **11**, 657 (2011).

[57] A. Kuzyk, R. Schreiber, Z. Fan, G. Pardatscher, E.M. Roller, A. Högele, F.C. Simmel, A.O. Govorov, and T. Liedl, Nature **483**, 311 (2012).

[58] P.K. Dutta, R. Varghese, J. Nangreave, S. Lin, H. Yan, and Y. Liu, J. Am. Chem. Soc. **133**, 11985 (2011).

[59] C.Y. Tseng and G. Zocchi, J. Am. Chem. Soc. **135**, 11879 (2013).

[60] L. Minghui, J. Fu, C. Christian, Y. Yang, N.W. Woodbury, K.V. Gothelf, Y. Liu, and H. Yan, Nat. Commun. **4**, 2127 (2013).

[61] O.I. Wilner, Y. Weizmann, R. Gill, O. Lioubashevski, R. Freeman, and I. Willner, Nat. Nanotechnol. **4**, 249 (2009).

[62] J. Fu, M. Liu, Y. Liu, N.W. Woodbury, and H. Yan, J. Am. Chem. Soc. **134**, 5516 (2012).

[63] J. Fu, Y.R. Yang, A. Johnson-Buck, M. Liu, Y. Liu, N.G. Walter, N.W. Woodbury, and H. Yan, Nat. Nanotechnol. **9**, 531 (2014).

[64] T.E. Tomov, R. Tsukanov, M. Liber, R. Masoud, N. Plavner, and E. Nir, J. Am. Chem. Soc. **135**, 11935 (2013).

[65] Y. Ke, S. Lindsay, Y. Chang, Y. Liu, and H. Yan, Science **319**, 180 (2008).

[66] H. Subramanian, B. Chakraborty, R. Sha, and N. Seeman, Nano Lett. **11**, 910 (2011).

[67] M. Endo, K. Tatsumi, K. Terushima, Y. Katsuda, K. Hidaka, Y. Harada, and H. Sugiyama, Angew. Chem. Int. Ed. **124**, 8908 (2012).

[68] E. Pfitzner, C. Wachauf, F. Kilchherr, B. Pelz, W.M. Shih, M. Reif, and H. Dietz, Angew. Chem. Int. Ed. **52**, 7766 (2013).

[69] N.D. Derr, B.S. Goodman, R. Jungmann, A.E. Lechziner, W.M. Shih, and S.L. Reck-Peterson, Science **338**, 662 (2012).

[70] S.M. Douglas, I. Bachelet, and G.M. Church, Science **335**, 831 (2012).

[71] R. Crawford, C.M. Erben, J. Periz, L.M. Hall, T. Brown, A.J. Turberfield, and A.N. Kapanidis, Angew. Chem. Int. Ed. **52**, 2284 (2013).

[72] J. Li, H. Pei, B. Zhu, L. Liang, M. Wei, Y. He, N. Chen, D. Li, Q. Huang, and C. Fan, ACS Nano **5**, 8783 (2011).

[73] V.J. Schüller, S. Heidegger, N. Sandholzer, P.C. Nickels, N.A. Suhartha, S. Endres, C. Bourquin, and T. Liedl, ACS Nano **5**, 9696 (2011).

[74] X. Liu, Y. Xu, T. Yu, C. Clifford, Y. Liu, H. Yan, and Y. Chang, Nano Lett. **12**, 4254 (2012).

[75] A.S. Walsh, H. Yin, C.M. Erben, M.J.A. Wood, and A.J. Turberfield, ACS Nano **5**, 5427 (2011).

[76] H. Lee, A.K.R. Lytton-Jean, Y. Chen, K.T. Love, A.I. Park, E.D. Karagiannis, A. Sehgal, W. Querbes, C.S. Zurenko, M. Jayaraman, C.G. Peng, K. Charisse, A. Borodovsky, M. Manoharan, J.S. Donahoe, J. Truelove, M. Nahrendorf, R. Langer, and D.G. Anderson, Nat. Nanotechnol. **7**, 389 (2012).

[77] Q. Mei, X. Wei, F. Su, Y. Liu, C. Youngbull, R. Johnson, S. Lindsay, H. Yan, and D. Meldrum, Nano Lett. **11**, 1477 (2011).

[78] S. Surana, D. Bhatia, and Y. Krishnan, Methods **64**, 94 (2013).

[79] S.D. Perrault and W.M. Shih, ACS Nano **8**, 5132 (2014).

[80] J. Mikkilä, A.P. Eskelinen, E.H. Niemelä, V. Linko, M.J. Frilander, P. Törmä, and M.A. Kostiainen, Nano Lett. **14**, 2196 (2014).

[81] Y. Amir, E. Ben-Ishay, D. Levner, S. Ittah, A. Abu-Horowitz, and I. Bachalet, Nat. Nanotechnol. **9**, 353 (2014).

[82] Y. He and D.R. Liu, Nat. Nanotechnol. **5**, 778 (2010).

[83] M.L. McKee, P.J. Milnes, J. Bath, E. Stulz, R.K. O'Reilly, and A.J. Turberfield, J. Am. Chem. Soc. **134**, 1446 (2012).

[84] H. Gu, J. Chao, S. Xiao, and N.C. Seeman, Nature **465**, 202 (2010).

[85] J.P.J. Sobczak, T.G. Martin, T. Gerling, and H. Dietz, Science **338**, 1458 (2012).

[86] C. Myhrvold, M. Dai, P.A. Silver, and P. Yin, Nano Lett. **13**, 4242 (2013).

[87] A. Reinhardt and D. Frenkel, Phys. Rev. Lett. **112**, 238103 (2014).

[88] J.M. Arbona, J. Elezgary, and J.P. Aimé, Europhys. Lett. **100**, 28006 (2012).

[89] Y. Ke, G. Bellot, N.V. Voigt, E. Fradkov, and W.M. Shih, Chem. Sci. **3**, 2587 (2012).

[90] T.G. Martin and H. Dietz, Nat. Commun. **3**, 1103 (2012).

[91] H. Chen, T.W. Weng, M.M. Riccitelli, Y. Cui, J. Irudayaraj, and J.H. Choi, J. Am. Chem. Soc. **136**, 6995 (2014).

[92] A. Johnson-Buck, J. Nangreave, S. Jiang, H. Yan, and N.G. Walter, Nano Lett. **13**, 2754 (2013).

[93] R. Tsukanov, T.E. Tomov, R. Masoud, H. Drory, N. Plavner, M. Liber, and E. Nir, J. Phys. Chem. B **117**, 11932 (2013).

[94] M. Teichmann, E. Kopperger, and F.C. Simmel, ACS Nano **8**, (2014).

[95] J. SantaLucia, Jr, and D. Hicks, Annu. Rev. Biophys. Biomol. Struct. **33**, 415 (2004).

[96] R.M. Dirks, J.S. Bois, J.M. Schaeffer, E. Winfree, and N.A. Pierce, SIAM Rev. **29**, 65 (2007).

[97] F. Oteri, M. Falconi, G. Chilemi, F.F. Andersen, C.L.P. Oliveira, J.S. Pedersen, B.R. Knudsen, and A. Desideri, J. Phys. Chem. C **168**, 11519 (2011).

[98] J. Yoo and A. Aksimentiev, Proc. Natl. Acad. Sci. USA **110**, 20099 (2013).

[99] N.B. Becker and R. Everaers, Phys. Rev. E **76**, 021923 (2007).
[100] N.B. Becker and R. Everaers, J. Chem. Phys. **130**, 135102 (2009).
[101] F. Lankaš, O. Gonzalez, L.M. Heffler, G. Stoll, M. Moakher, and J.H. Maddocks, Phys. Chem. Chem. Phys. **11**, 10565 (2009).
[102] M. Sayar, B. Avşaroğlu, and A. Kabakçıoğlu, Phys. Rev. E **81**, 041916 (2010).
[103] A. Savelyev and G.A. Papoian, Proc. Natl. Acad. Sci. U.S.A **107**, 20340 (2010).
[104] P.D. Dans, A. Zeida, M.R. Machado, and S. Pantano, J. Chem. Theory Comput. **6**, 1711 (2010).
[105] A. Morriss-Andrews, J. Rottler, and S.S. Plotkin, J. Chem. Phys. **132**, 035105 (2010).
[106] I.P. Kikot, A.V. Savin, E.A. Zubova, M.A. Mazo, E.B. Gusarova, L.I. Manevitch, and A.V. Onufriev, Biophysics **56**, 387 (2011).
[107] A.V. Savin, M.A. Mazo, I.P. Kikot, L.I. Manevitch, and A.V. Onufriev, Phys. Rev. B **83**, 245406 (2011).
[108] O. Gonzalez, D. Petkevičiutė, and J.H. Maddocks, J. Chem. Phys. **138**, 055102 (2013).
[109] Y. He, M. Maciejczyk, S. Ołdziej, H.A. Scheraga, and A. Liwo, Phys. Rev. Lett. **110**, 098101 (2013).
[110] N.A. Kovaleva, I.P. Kikot, M.A. Mazo, and E.A. Zubova, arXiv:1401.2770 (2014).
[111] C. Maffeo, T.T.M. Ngo, T. Ha, and A. Aksimentiev, J. Chem. Theory Comput. **10**, 2891 (2013).
[112] N. Korolev, D. Luo, A.P. Lyubartsev, and L. Nordenskiöld, Polymers **6**, 1655 (2014).
[113] A. Naômé, A. Laasksonen, and D.P. Vercauteren, J. Chem. Theory Comput. **10**, 3541 (2014).
[114] W.K. Olson, A.A. Gorin, X.J. Lu, L.M. Hock, and V.B. Zhurkin, Proc. Natl. Acad. Sci. U.S.A. **95**, 11163 (1998).
[115] F. Trovato and V. Tozzini, J. Phys. Chem. B **112**, 13197 (2008).
[116] M.E. Johnson, T. Head-Gordon, and A.A. Louis, J. Chem. Phys. **126**, 144509 (2007).
[117] C.W. Hsu, M. Fyta, G. Lakatos, S. Melchionha, and E. Kaxiras, J. Chem. Phys. **137**, 105102 (2012).
[118] K. Drukker, G. Wu, and G.C. Schatz, J. Chem. Phys. **114**, 579 (2001).
[119] M. Sales-Pardo, R. Guimera, A.A. Moreira, J. Widom, and L. Amaral, Phys. Rev. E **71**, 051902 (2005).
[120] F.W. Starr and F. Sciortino, J. Phys.: Condens. Matter **18**, 347 (2006).
[121] N.B. Tito and J.M. Stubbs, Chem. Phys. Lett. **485**, 354 (2010).
[122] T.A. Knotts, IV, N. Rathore, D. Schwartz, and J.J. de Pablo, J. Chem. Phys. **126** 084901 (2007).
[123] E.J. Sambriski, D.C. Schwartz, and J.J. de Pablo, Biophys. J. **96**, 1675 (2009).
[124] D.M. Hinckley, G.S. Freeman, J.K. Whitmer, and J.J. de Pablo, J. Chem. Phys. **139**, 144903 (2013).
[125] C. Svaneborg, Comput. Phys. Commun. **183**, 1793 (2012).
[126] M. Kenward and K.D. Dorfman, J. Chem. Phys. **130**, 095101 (2009).
[127] M.C. Linak, R. Tourdot, and K.D. Dorfman, J. Chem. Phys. **135**, 205120 (2011).
[128] J.C. Araque, A.Z. Panagiotopoulos, and M.A. Robert, J. Chem. Phys. **134**, 165103 (2011).
[129] S. Niewieczerzał and M. Cieplak, J. Phys.: Condens. Matter **21**, 474221 (2009).
[130] J.M. Arbona, J.P. Aimé, and J. Elezgaray, Phys. Rev. E **86**, 051912 (2012).
[131] L.E. Edens, J.A. Brozik, and D.J. Keller, J. Phys. Chem. B **116**, 14735 (2012).
[132] A.K. Dasanna, N. Destainville, J. Palmeri, and M. Manghi, Phys. Rev. E **87**, 052703 (2013).
[133] T. Cragnolini, P. Derreumaux, and S. Pasquali, J. Phys. Chem. B **117**, 8047 (2013).
[134] K. Doi, T. Haga, H. Shintaku, and S. Kawano, Philos. Trans. R. Soc. A **368**, 2615 (2010).
[135] S.P. Mielke, N. Gronbech-Jensen, V.V. Krishnan, W.H. Fink, and C.J. Benham, J. Chem. Phys. **123**, 124911 (2005).
[136] C. Knorowski, S. Burleigh, and A. Travesset, Phys. Rev. Lett. **106**, 215501 (2011).
[137] T.E. Ouldridge, A.A. Louis, and J.P.K. Doye, J. Chem. Phys. **134**, 085101 (2011).
[138] T.E. Ouldridge, Ph.D. thesis, University of Oxford, 2011 [published as a book by Springer, Heidelberg, 2012].
[139] P. Šulc, F. Romano, T.E. Ouldridge, L. Rovigatti, J.P.K. Doye, and A.A. Louis, J. Chem. Phys. **137**, 135101 (2012).
[140] J.H. Allen, E.T. Schoch, and J.M. Stubbs, J. Phys. Chem. B **115**, 1720 (2011).
[141] T.R. Prytkova, I. Eryazici, B. Stepp, S. Nguyen, and G.C. Schatz, J. Phys. Chem. B **114**, 2627 (2010).
[142] M.J. Hoefert, E.J. Sambriski, and J.J. de Pablo, Soft Matter **7**, 560 (2011).
[143] T.J. Schmitt, B. Rogers, and T.A. Knotts IV, J. Chem. Phys. **138**, 035102 (2013).
[144] D. Hinckley, J.P. Lequieu, and J.J. de Pablo, J. Chem. Phys. **141**, 035102 (2014).
[145] F.B. Bombelli, F. Gambinossi, M. Lagi, D. Berti, G. Caminati, T. Brown, F. Sciortino, B. Norden, and P. Baglioni, J. Phys. Chem. B **112**, 15283 (2008).
[146] J.M. Arbona, J.P. Aimé, and J. Elezgaray, J. Chem. Phys. **136**, 065102 (2012).
[147] C. Svaneborg, H. Fellermann, and S. Rasmussen, in *DNA Computing and Molecular Programming*, edited by D. Stefanovic and A.J. Turberfield (Springer, Berlin Heidelberg, 2012), Vol. 7433, pp. 123–134.
[148] T.E. Ouldridge, I.G. Johnston, A.A. Louis, and J.P.K. Doye, J. Chem. Phys. **130**, 065101 (2009).
[149] C. Svaneborg, H. Fellerman, and S. Rasmussen, arxiv1210.6156 (2012).
[150] T.I. Li, R. Sknepnek, R.J. Macfarlane, C.A. Mirkin, and M.O. de la Cruz, Nano Lett. **12**, 2509 (2012).
[151] C. Hyeon and D. Thirumalai, Proc. Natl. Acad. Sci. U.S.A. **102**, 6789 (2005).
[152] A. Cao and S.J. Chen, Nucl. Acids Res. **34**, 2634 (2006).
[153] D. Jost and R. Everaers, J. Chem. Phys. **132**, 095101 (2010).
[154] F. Ding, S. Sharma, P. Chalasani, V.V. Demidov, N.E. Broude, and N.V. Dokholyan, RNA **14**, 1164 (2008).
[155] S. Pasquali and P. Derreumaux, J. Phys. Chem. B **114**, 11957 (2010).
[156] A. Dickson, M. Maienschein-Cline, A. Tovo-Dwyer, J.R. Hammond, and A.R. Dinner, J. Chem. Theory Comput. **7**, 2710 (2011).
[157] N.A. Denesyuk and D. Thirumalai, J. Phys. Chem. B **117**, 4901 (2013).
[158] M.A. Jonikas, R.J. Radmer, A. Laederach, R. Das, S. Pearlman, D. Herschlag, and R.B. Altman, RNA **15**, 189 (2009).
[159] R. Das and D. Baker, Proc. Natl. Acad. Sci. U.S.A **104**, 14664 (2009).
[160] M. Paliy, R. Melnik, and B.A. Shapiro, Phys. Biol. **7**, 036001 (2010).

[161] Z. Xia, D.R. Bell, Y. Shi, and P. Ren, J. Phys. Chem. B **117**, 3135 (2013).
[162] S. Whitelam, E.H. Feng, M.F. Hagan, and P.L. Geissler, Soft Matter **5**, 1251 (2009).
[163] R.L. Davidchack, R. Handel, and M.V. Tretyakov, J. Chem. Phys. **130**, 234101 (2009).
[164] J. Russo, P. Tartaglia, and F. Sciortino, J. Chem. Phys. **131**, 014504 (2009).
[165] G.M. Torrie and J.P. Valleau, J. Comp. Phys. **23**, 187 (1977).
[166] R.J. Allen, P.B. Warren, and P.R. ten Wolde, Phys. Rev. Lett. **94**, 018104 (2005).
[167] R.J. Allen, C. Valeriani, and P.R. ten Wolde, J. Phys.: Condens. Matter **21**, 463102 (2009).
[168] Q. Wang and B.M. Pettitt, Biophys. J. **106**, 1182 (2014).
[169] T.E. Ouldridge, J. Chem. Phys. **137**, 144105 (2012).
[170] R.R.F. Machinek, T.E. Ouldridge, N.E.C. Haley, J. Bath, and A.J. Turberfield, Nat. Commun. (In Press).
[171] A.J. Genot, D.Y. Zhang, J. Bath, and A.J. Turberfield, J. Am. Chem. Soc. **133**, 2177 (2011).
[172] D.Y. Zhang, S.X. Chen, and P. Yin, Nat. Chem. **4**, 208 (2012).
[173] Y.S. Jiang, S. Bhadra, B. Li, and A.D. Ellington, Angew. Chem. Int. Ed. **126**, 1876 (2014).
[174] Q. Li, G. Luan, Q. Guo, and J. Liang, Nucl. Acids Res. **30**, e5 (2002).
[175] D.Y. Zhang, S.X. Chen, and Y. Peng, Nat. Chem. **4**, 208 (2012).
[176] S.X. Chen, D.Y. Zhang, and G. Seelig, Nat. Chem. **5**, 782 (2013).
[177] P. Šulc, T.E. Ouldridge, F. Romano, J.P.K. Doye, and A.A. Louis, Nat. Comput. 1–13 (2013).
[178] T.E. Ouldridge, R.L. Hoare, A.A. Louis, J.P.K. Doye, J. Bath, and A.J. Turberfield, ACS Nano **7**, 2479 (2013).
[179] H. Qu, Y. Wang, C.Y. Tseng, and G. Zocchi, Phys. Rev. X **1**, 021008 (2011).
[180] J. Wang, H. Qu, and G. Zocchi, Phys. Rev. E **88**, 032712 (2013).
[181] Y. Li, C. Zhang, C. Tian, and C. Mao, Org. Biomol. Chem. **12**, 2543 (2014).
[182] J.R. Sikora, B. Rauzan, R. Stegemann, and A. Deckert, J. Phys. Chem. B **117**, 8966 (2013).
[183] T.E. Ouldridge, P. Šulc, F. Romano, J.P.K. Doye, and A.A. Louis, Nucl. Acids Res. **41**, 8886 (2013).
[184] P.A. Wiggins, T. van der Heijden, F. Moreno-Herrero, A. Spakowitz, R. Phillips, J. Widom, C. Dekker, and P.C. Nelson, Nat. Nanotechnol. **1**, 137 (2006).
[185] R. Vafabakhsh and T. Ha, Science **337**, 1097 (2012).
[186] A. Vologodskii and M.D. Frank-Kamenetskii, Nucl. Acids Res. **41**, 6785 (2013).
[187] A.K. Mazur and M. Maaloum, Phys. Rev. Lett. **112**, 068104 (2014).
[188] J.P.K. Doye, T.E. Ouldridge, A.A. Louis, F. Romano, P. Šulc, C. Matek, B. Snodin, L. Rovigatti, J.S. Schreck, R.M. Harrison, and W.P.J. Smith, Phys. Chem. Chem. Phys. **15**, 20395 (2013).
[189] L. Rovigatti, F. Smallenburg, F. Romano, and F. Sciortino, ACS Nano **8**, 3567 (2014).
[190] L. Rovigatti, F. Bomboi, and F. Sciortino, J. Chem. Phys. **140**, 154903 (2014).
[191] P. Šulc, F. Romano, T.E. Ouldridge, J.P.K. Doye, and A.A. Louis, J. Chem. Phys. **140**, 235102 (2014).
[192] J. Schaeffer, Ph.D. thesis, California Institute of Technology, 2013.
[193] A. Phillips and L. Cardelli, J. R. Soc. Interface **6**, S419 (2009).